Current noise in barrier photoconducting devices (II. Experiment)

Current noise in barrier photoconducting devices. II. Experiment

A. Carbone and P. Mazzetti
Dipartimento di Fisica del Politecnico di Torino, C.so Duca degli Abruzzi 24, 10129 Torino, Italy
(Received 16 August 1993)

Many measurements of photocurrent noise and of other quantities related to the photoconduction processes were performed on CdS based devices to check the theory of current noise, developed on the basis of a barrier-type model of the photoconduction mechanism in the preceding paper. Noise power spectrum measurements have been carried out in a wide range of photon flux densities ($8\times10^{10}\leq\phi_{n_f}\leq2\times10^{13}$ photons $s^{-1}cm^{-2}$) as a function of light wavelength in the range between 400 and 750 nm. The most interesting feature of these results is the abrupt variation of the noise power spectrum occurring in correspondence with the critical wavelength λ_{gap}, even if the device conductance is kept constant by varying the light intensity. Measurements concerning the behavior of the photoconductance, the optical transmittance, and the photoresponsivity versus light intensity and wavelength were also taken and used to determine most of the parameters appearing in the theoretical expression of the noise power spectrum. The relative variations of the shape and amplitude of the noise power spectra with light intensity and wavelength are reproduced by the theory without introduction of free parameters. Also the absolute value of the noise power spectrum at medium to high illumination value ($\phi_{n_f}>10^{11}$ photons $s^{-1}cm^{-2}$) and at frequencies below 5 kHz, where the photoinduced noise component dominates, is reproduced by the theory without free parameters. Finally, by assuming a suitable value of the parameter τ_s appearing in the distribution function of the free-electron lifetimes and representing the inverse of the cutoff angular frequency of the g-r Lorentzian component, the whole set of experimental results is completely fitted by the theory for any value of the light intensity and wavelength, in the explored range.

I. INTRODUCTION

In this paper we report a consistent set of experimental results taken on a CdS based photoconducting device in order to check the theory of current noise developed in the preceding paper (Paper I).[7] Some of these results, concerning the behavior of photoconductance versus light intensity, have already been used in Appendix B of Paper I to support the barrier-type photoconduction model used to develop the noise theory. In the following, reference to equations of Paper I will be made by inserting a I in the equation number.

In order to have a self-consistent set of values of the quantities appearing in the analytical expression of the noise power spectrum, all measurements were performed on the same device: a CdS based photoconducting film with indium Ohmic contacts,[1] set inside an evacuated glass container. Very similar results were obtained on other CdS and CdSe based devices, but they are not reported here.[2] The results reported in Secs. II–IV concern the following measurements: (a) photoconductance noise power spectra; (b) photoconductance, photoresponsivity, and photocurrent relaxation; and (c) optical transmittance.

All these measurements have been carried out using monochromatic light at different wavelengths above and below the critical wavelength λ_{gap}, corresponding to the energy gap of the photoconducting material ($\lambda_{gap}=500$ nm for CdS). Light intensity was also changed in a wide range of values corresponding to three orders of magnitude of the device conductance.

Most of the parameters entering the expression of the photoconductance noise power spectrum at different light intensities and wavelengths are provided by these measurements, which also represent a test of the photoconduction model on which the theory is based. For instance, the behavior of photoconductance versus light intensity is in good agreement with a barrier photoconduction mechanism, as discussed in Appendix B of Paper I.

It will be shown that the relative variations of the photoconductance noise power spectrum are reproduced by the theory without free parameters when the wavelength and the intensity of the light are varied. The absolute value of the noise power spectrum, as a function of both light wavelength and intensity, can also be accounted for by the theory without free parameters in the low-frequency range ($f<5$ kHz) where the photoinduced noise component, defined in Paper I, dominates the power spectrum (photon flux density $\Phi_{n_f}>10^{11}$ photons $s^{-1}cm^{-2}$).

At higher frequencies or at lower light intensities, the noise power spectrum is influenced by the intrinsic component, whose evaluation requires the knowledge of the parameter ω_c characterizing the lifetime distribution function of free electrons [Eq. (I3.2)]. This situation is described in detail in Sec. IV.

In the following sections, after a brief description of the experimental setup and of the equivalent circuit used to obtain the correct photoconductance fluctuation spectra, results concerning the measurements listed above are

reported. Finally, a discussion of these results and a comparison with the theoretical ones are given.

II. EXPERIMENTAL SETUP

Measurements were performed on an Ag-doped, CdS-based photoconducting film, approximately 1.5 μm thick, deposited on a glass substrate with indium Ohmic coplanar contacts set about 1 mm apart and enclosed in an evacuated glass container. Dark electric conductance was about $4\times10^{-10}S$ and can be disregarded in the reported measurements, in which photoconductance values range from $2\times10^{-8}S$ to $10^{-4}S$.

The experimental setup is sketched in Fig. 1(a). Parasitic capacities were determined by injecting a variable frequency ac electric signal into the photoconducting device and by measuring the transfer function of the output voltage of the preamplifier. Voltage noise power spectra, as well as frequency transfer functions, were detected by means of a two-channel signal analyzer (Hewlett Packard Model 3562A) on the resistor R_1.

The equivalent circuit reported in Fig. 1(b) has been used to correct the measured quantities both in the frequency and in the time domain. The equivalent circuit has also provided the relationship between the photoconductance noise power spectrum $\Phi_G(f)$ and the voltage noise power spectrum $\Phi_V(f)$ at the preamplifier input:

$$\frac{\Phi_G(f)}{G^2}=\frac{(R_0+R_e)^2}{R_0^2}\left[1+\frac{(2\pi f)^2C_e^2R_0^2R_e^2}{(R_0+R_e)^2}\right]\frac{\Phi_V(f)}{V^2}\,. \tag{2.1}$$

In this equation, G is the average photoconductance, V is the voltage drop at the ends of R_e, and the other quantities are given in Fig. 1.

The introduction of the photoconductance noise power spectrum $\Phi_G(f)$ is justified by the fact that $\Phi_V(f)$ turns out to be proportional to the square of the bias current in the whole range of values used in the present set of measurements. This means that the photocurrent noise is actually due to conductance fluctuation processes. The quantity $\Phi_G(f)/G^2$, which represents the relative photoconductance fluctuation power spectrum, will be briefly indicated with $\psi_G(f)$. To compare experimental and theoretical results, it has been taken into account that the theoretical power spectrum $\Phi_G(\omega)$, as defined in Paper I, is equal to $(1/4\pi)\Phi_G(f)$. Actually, $\Phi_G(f)$, as given by the signal analyzer, contains the frequency f instead of ω and is defined only for positive values of this quantity.

A halogen lamp has been used as a bias light source. It was connected to a regulated dc power supply and collimated to the input slit of a monochromator having a resolution of about 3 nm at the maximum slit width used. Light was aimed to the photoconductor by an optical waveguide connected to the output slit of the monochromator. Light-intensity measurements were obtained by means of a calibrated photocell (EG&G model 444BQ). Light-intensity fluctuations in excess to the normal shot noise were confirmed to be very limited, as shown in Fig. 2, which gives the power spectrum of the current noise in a saturated vacuum photodiode (Gillod-Boutry) put in place of the photoconductor in the experimental setup.

Photocurrent relaxation measurements were performed by adding to the main light source a short (about 10^{-6} s) light pulse produced by a xenon lamp. Photocurrent relaxation pulses were then stored in a digital oscilloscope. The nonexponential behavior of these pulses was interpreted, according to the photoconduction model developed in Paper I, as a superposition of exponential decays having different amplitude and relaxation time.

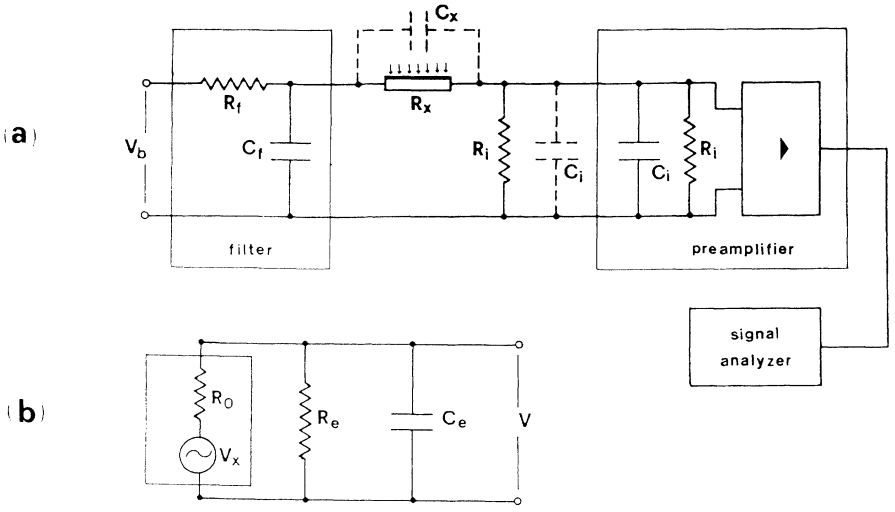

FIG. 1. (a) Schematic diagram of the experimental setup: R_x and C_x represent, respectively, the average resistance and capacity of the photoconductor; R_1 is the load resistor and C_1 its parasitic capacity. R_i and C_i are, respectively, the input resistance and capacity of the preamplifier. Light is sent to the photoconductor through an optical waveguide connected to the output slit of a monochromator. (b) Noise equivalent circuit: $C_e=C_x+C_1+C_i$ is the input equivalent capacity, $R_e=R_1R_i/(R_1+R_i)$ is the equivalent load resistance, and $R_0=\langle R_x\rangle$ is the average photoconductor resistance. This circuit has been used to obtain and to correct the conductance fluctuation power spectrum up to a frequency of 100 kHz [see Eq. (2.1)].

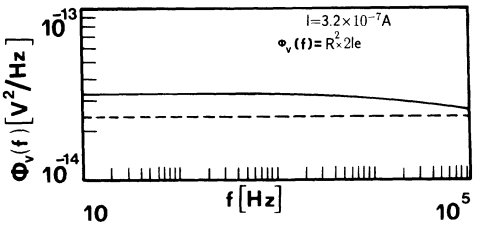

FIG. 2. Shot-noise power spectrum of a saturated Gillod-Boutry vacuum photodiode illuminated by the same monochromatic light used to excite the CdS photoconductor. I is the photocurrent; V is the voltage drop at the ends of R, in series with the photodiode; $\Phi_V(f)$ the power spectrum of V; and e is the electron charge. The dotted line is the theoretical spectrum. The negligible deviation of the experimental spectrum from the theoretical one shows that the light source is practically free of any excess noise in the range of frequencies used to detect photoconduction noise spectra.

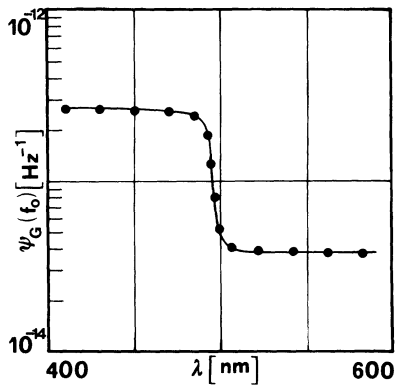

FIG. 3. Power spectral density of the relative conductance noise $\psi_G(f_0)=\Phi_G(f_0)/G^2$ versus photon wavelength λ at $f_0=200$ Hz. G is kept constant at the value $2\times10^{-5}S$ when λ is varied, by adjusting the light intensity. The abrupt change of the power spectral density occurs at $\lambda=\lambda_{gap}$, which corresponds to the energy gap of the photoconductor ($\lambda_{gap}=500$ nm for CdS).

The amplitude distribution of these exponentials appears in the theoretical power spectrum [Eq. (I3.34)]. It could be obtained by fitting the relaxation pulse with a superposition of exponentials, but a more precise evaluation was achieved by the photoresponse measurement, as described in Sec. IV. These measurements were carried out, as described below, by superimposing a small ac optical signal to the main light source. Part of the monochromatic light impinging on the photoconductor was sent, by means of a beam splitter, to a photomultiplier (RCA model C31034A-02) having a flat response to modulated light up 1 MHz. The outputs of the photomultiplier and of the photoconducting device (preamplifier output of Fig. 1) were sent to the signal analyzer, which directly gives the transfer function at each frequency value independently of the signal wave form.

III. RESULTS

First, we will present some general results concerning the behavior of the relative photoconductance noise power spectrum $\psi_G(f)$ as a function of light intensity and wavelength. Data concerning the photoconductance, photoresponsivity, optical transmittance, etc., of the same specimen, needed to obtain the essential parameters entering the theory of the current noise developed in Paper I, will be given subsequently.

As already mentioned, one of the most interesting aspects of the photoconductance noise power spectrum is its abrupt change when the light wavelength takes values just across λ_{gap} and the average conductance value G is kept constant by adjusting the light intensity. This change, which is one order of magnitude large at frequencies near 1 kHz, is shown in Fig. 3 for the CdS sample on which all other reported measurements were performed. The power spectrum remains practically unchanged for wavelengths shorter than 490 nm or longer than 510 nm. This behavior has been found in all studied CdS or CdSe based samples, even if the slope of the curve representing the power spectral density as a function of λ in correspondence with λ_{gap} depends on the material.[2] The theory developed in Paper I is successful in reproducing this effect, as will be shown later in more detail.

Since nearly the whole change of power spectrum occurs between $\lambda=510$ and 490 nm, all the experimental results are given for these two values of the light wavelength. Typical photoconductance noise power spectra are reported in Figs. 4 (high light intensity) and 5 (low light intensity), with the corresponding theoretical spectra (solid lines). As discussed in Sec. IV, the theoretical spectra are calculated from Eq. (I3.34) on the basis of the data exerimentally obtained under the same physical conditions.

As shown in Paper I and discussed in detail in Sec. IV, two noise components, a photoinduced and an intrinsic component, may be envisaged in the power spectrum. They can be distinguished by looking at the change of the shape of the power spectrum as the light intensity is varied. At high light intensity the spectrum is dominated, in the low-frequency range, by the photoinduced component, which has a nearly Lorentzian shape. At low light intensities, where the photoinduced noise component becomes negligible with respect to the intrinsic one, the power spectrum becomes $1/f$ shaped in the low-frequency range. A dependence on λ of the power spectrum can also be observed in the low-frequency range, both at high (Fig. 4) and at low light intensity (Fig. 5). According to the theory, such a dependence can be related to an abrupt change of the photocurrent relaxation time when λ crosses λ_{gap}. By measuring this variation of the relaxation time and introducing it in the theoretical expression of the power spectrum, as described in Sec. IV, a good agreement between theory and experiment is found without the introduction of any adjustable parameter.

At very low light intensity, when the photoinduced noise component becomes negligible with respect to the $1/f$ component, the effect is smaller and is mostly due to the increase of this last component. Actually, for

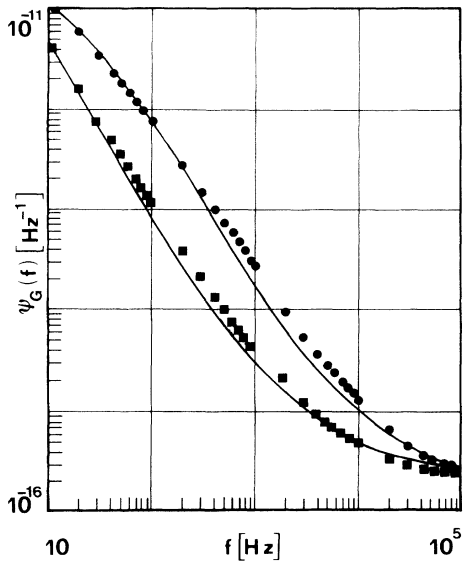

FIG. 4. Power spectra of the relative conductance fluctuation noise $\psi_G(f)$ taken at $\lambda=490$ nm (●) and at $\lambda=510$ nm (■). The average electrical conductance ($G=2\times10^{-5}S$) is the same for both spectra and corresponds to rather high photon flux densities (respectively, 4×10^{12} and 1.1×10^{13} photons s^{-1} cm^{-2}). The points are experimental and correspond to local averages of the plotted curves over several runs. The standard deviation is less than 10%. The solid lines are theoretical from Eq. (4.1). The values of the quantities n_d and Δ_g, which depend on G, were obtained from the data reported in Figs. 14 and 15. The other constant quantities and the $\tau_d^{(j)}$ distribution are given in Sec. IV and in Table I. The approximately $1/f^2$ behavior at low frequencies indicates the predominance of the photoinduced noise component.

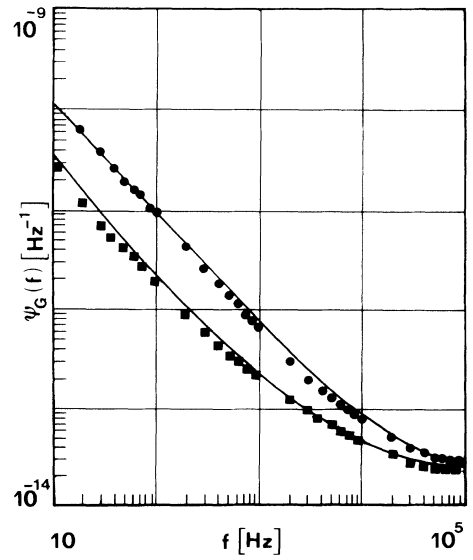

FIG. 5. The same as Fig. 4, except that the spectra refer to a much lower light intensity. The average conductance is now $G=2\times10^{-7}S$. The $1/f$ behavior at low frequencies indicates that the contribution of the photoinduced noise component has become negligible and the intrinsic noise component is dominating the whole spectrum.

$\lambda<\lambda_{gap}$, the light absorption coefficient becomes extremely high and the electrical conduction occurs near the photoconductor surface, which is the main source of the $1/f$ noise. In this case the quantity ω_c, characterizing the electron lifetime distribution function given by Eq. (3.2), is used as an adjustable parameter to get the curves reported in Fig. 5. This parameter, which cannot be directly measured on the device, turns out to be independent of the light intensity.

A more extended set of data concerning the behavior of the relative conductance noise power spectral density $\psi_G(f_0)$ as a function of the photoconductance G for different values of the frequency f_0 are given in Figs. 6 and 7. It can be seen that the high-frequency spectral density, which is dominated by the intrinsic noise component, drops nearly as $1/G$, as expected. However, at low frequencies, particularly for $\lambda<\lambda_{gap}$, the drop is slower due to the increasing effect of the photoinduced component, the contribution of which increases as G increases.

It can be observed, comparing Figs. 6 and 7, that the high-frequency power spectral density does not depend on λ when G is kept constant. This is shown in Figs. 4 and 5, where full spectra are reported. According to the theory, this is related to the fact that in the high-frequency part of the spectrum, the *g-r* noise, which does

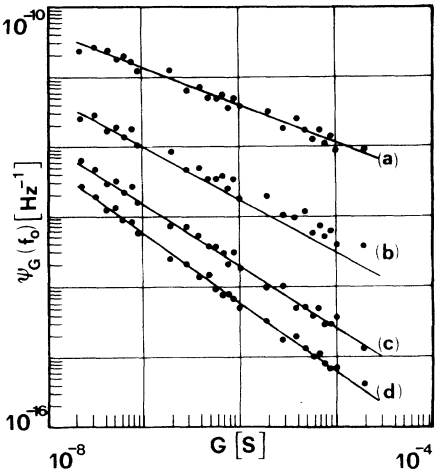

FIG. 6. Power spectral density of the relative conductance fluctuation noise $\psi_G(f_0)$ versus conductance G taken at a constant value of the light wavelength ($\lambda=490$ nm), slightly below the critical value λ_{gap}. The different curves are relative to different values of the analysis frequency [(a) $f_0=100$ Hz, (b) $f_0=1$ kHz, (c) $f_0=10$ kHz, and (d) $f_0=100$ kHz]. The experimental points are local averages of the plotted spectra over single runs and the standard deviation is higher than the one relative to the data of Figs. 4 and 5, as it appears from the larger spread of the points. The solid lines are theoretical and are derived from Eq. (4.1). The values of n_d and Δg, which depend on G, were obtained from the data reported in Figs. 14 and 15. The other parameters were obtained experimentally as described in Sec. IV. The high-frequency spectral density, which is dominated by the intrinsic noise component, drops as $1/G$, while the low-frequency one drops more slowly, due to the increasing contribution of the photoinduced noise component.

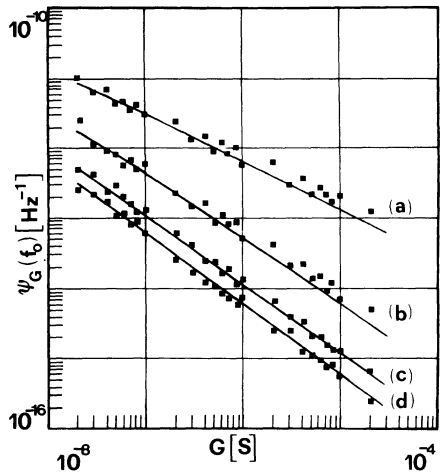

FIG. 7. The same as Fig. 6 but for $\lambda=510$ nm, slightly above λ_{gap}. The curves are steeper and closer to each other than those of Fig. 6, since in this case the contribution of the photoinduced component, which increases accordingly to the light intensity, is smaller (see Figs. 4 and 5).

not depend on λ, becomes the dominant component. The theoretical results are shown in the same figures (solid lines) and are in good agreement with the experimental ones.

Figure 8 represents the behavior of the photoconductance versus the photon flux impinging on the effective area of the device for two different λ values immediately below and above the critical wavelength λ_{gap}. These curves show a dependence on the photon flux, in agreement with a barrier-type conduction mechanism. They have been quantitatively accounted for in Appendix B of Paper I. It can be noticed that the ratio between the photon flux at $\lambda=510$ nm and at $\lambda=490$ nm, corresponding to the same value of the photoconductance, remains practically constant (equal to about 3.2) as light intensity is varied. As shown in the following, the same photon flux produces a larger photoconductance at $\lambda=510$ nm than at $\lambda=490$ nm because the relaxation time of the photocurrent has an abrupt increase when the light wavelength becomes larger than λ_{gap}. Actually, according to the model, in the first case the relaxation time is related to recombination of ionized donor centers, while in the second one it is related to recombination of trapped holes.

To simplify the forthcoming discussion, Eq. (I3.6), giving the average number n_d of ionized deep donor centers, is reported here:

$$n_d=\sum_j n^{(j)}=\eta_\lambda n_f \sum_j b^{(j)}\tau_d^{(j)}=\eta_\lambda n_f \tau_d \ . \tag{3.1}$$

In this equation, η_λ is the average quantum efficiency defined by Eq. (I3.25), $b^{(j)}$ is the ratio of the number of j center ionizations to the total ionization processes produced per unit time, n_f is the photon flux, $\tau_d^{(j)}$ is the average relaxation time of the j centers, and $\tau_d=\sum_j b^{(j)}\tau_d^{(j)}$ is an average relaxation time produced by a small pulse of light superimposed to the bias light.

Figure 14 shows that, as expected from the barrier photoconduction model, the same conductance value is obtained with the same value of n_d. Since τ_d is about one order of magnitude larger at $\lambda=510$ nm than at $\lambda=490$ nm (see Fig. 13), it turns out that $\eta_{510}\simeq 0.27\eta_{490}$. The curves reported in Fig. 8, taking into account the results of Fig. 13, also show that the ratio between the two efficiency factors is independent of the light intensity over an extended range of conductance values, covering about three decades, a result which is also in good agreement with the model. For $\lambda=490$ nm, where the light absorption is nearly total (see Fig. 10), the value of η_{490} was further assumed to be close to unity.

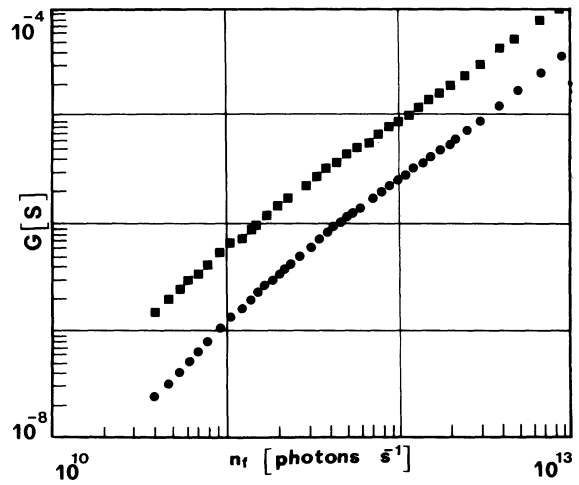

FIG. 8. The electrical conductance G versus photon flux n_f at $\lambda=510$ nm (■) and at $\lambda=490$ nm (●). The behavior is superlinear at low light intensity and linear at high light intensity. Statistical errors are of the order of the dots' dimensions, while accuracy in the evaluation of the photon flux impinging on the active area of the device is limited to ±20%.

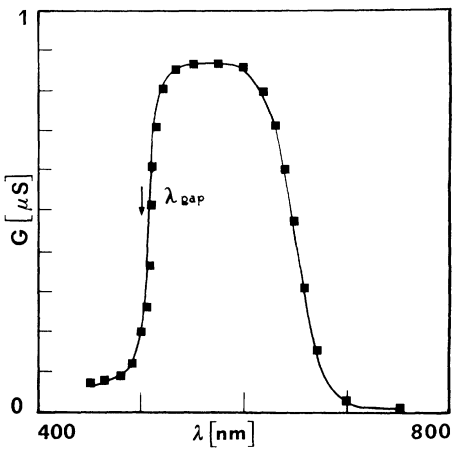

FIG. 9. The electrical conductance G versus light wavelength λ at a fixed value of photon flux n_f ($n_f\cong 10^{11}$ photons s^{-1}). According to the barrier model, the rapid increase of the conductance with λ in correspondence of λ_{gap} is mostly related to a corresponding rapid increase of the lifetime of the positive trapped charge (see Fig. 13) which controls the barrier height (trapped holes for $\lambda<\lambda_{gap}$, deep donor centers for $\lambda>\lambda_{gap}$).

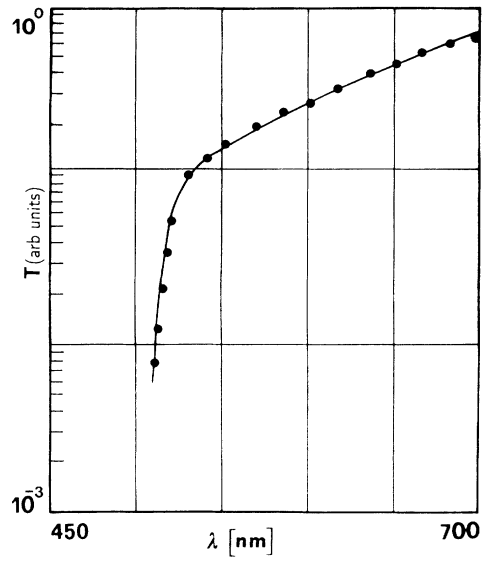

FIG. 10. Relative variation of the optical transmittance T as a function of wavelength λ. The strong light absorption for $\lambda < \lambda_{gap}$ is the origin of the fact that electrical conduction becomes mostly localized at the photoconductor surface and produces an enhancement of the $1/f$ noise component.

The behavior of the photoconductance versus the light wavelength at constant photon flux is represented in Fig. 9. This figure shows that a large photoconductance change occurs when λ equals the critical wavelength λ_{gap}. The decrease of photoconductance at wavelengths larger than 600 nm is due to the fact that the absorption coefficient and the quantum efficiency keep on decreasing,[3] while the mean lifetimes are practically unchanged, as experimentally found.

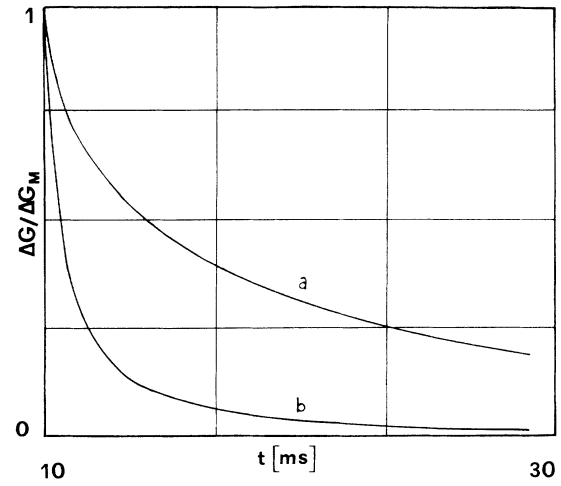

FIG. 11. Normalized phototransient decay curves obtained after a light pulse about 10^{-5} s long, superimposed to a background light source, at $\lambda = 510$ nm (a) and at $\lambda = 490$ nm (b). The curves are not simple exponential functions and are interpreted as a superposition of exponential decays related to the different lifetimes of the ionized centers or trapped holes (according to the λ value) which control the barrier height. The average conductance G is the same for the two curves and corresponds to $10^{-6}S$.

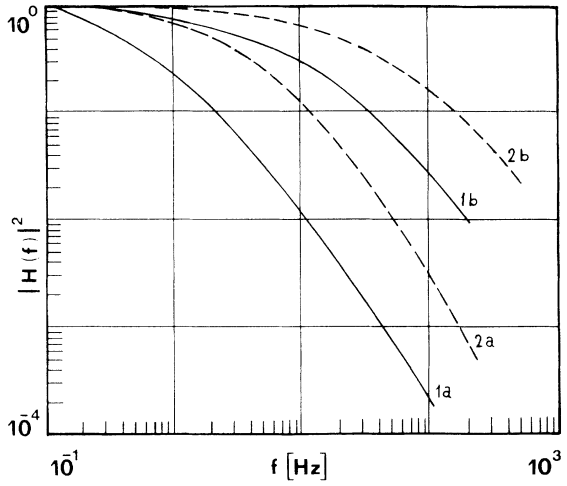

FIG. 12. Normalized photoresponse at $\lambda = 510$ nm (curves 1a) and 2a) and at $\lambda = 490$ nm (curves 1b and 2b) for two different values of the conductance G: $10^{-6}S$ (dashed lines) and $10^{-7}S$ (solid lines), respectively. The curves were obtained by superimposing to the background light, which determines the value of G, a small sinusoidal light signal of variable frequency and using a two-channel analyzer and the technique described in Sec. II to measure the transfer function. The set of $\tau_d^{(j)}$ and $a^{(j)}$ values used to obtain the theoretical spectra given in Figs. 4–7 were obtained by similar curves using an interpolation procedure.

The optical transmittance T is shown in Fig. 10. The curve of T versus λ could be taken, as all the other measurements reported here, on the same photoconducting device, which noise spectra refer to, thanks to the transparency of the glass substrate on which the film was

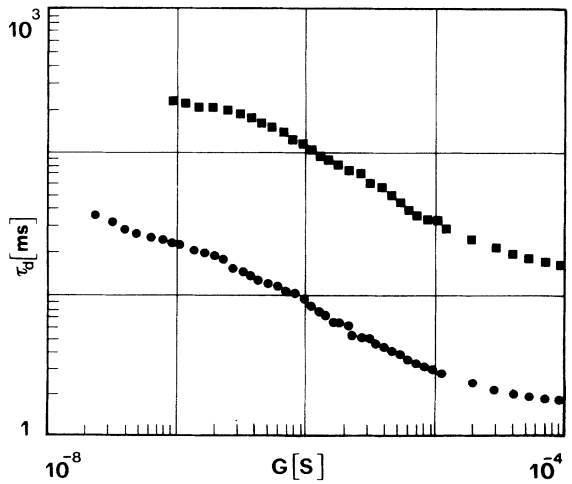

FIG. 13. The average decay time τ_d of the photocurrent at $\lambda = 490$ nm (●) and at $\lambda = 510$ nm (■) versus conductance G. The curves were obtained from a set of measurements of the type reported in Fig. 11, as described in the text. Estimated errors are approximately represented by the dots' dimensions. The conductance G has been varied by changing the intensity of the background monochromatic light.

deposited. To obtain τ_d and the distribution of the lifetimes $\tau_d^{(j)}$'s relative to the different kinds of donor centers, measurements concerning the photoconductance relaxation after a brief pulse of light and the photoresponse of the device to small sinusoidal light signals in the low-frequency range were carried out with the technique briefly described in Sec. II. Figures 11 and 12 show some typical results. By performing these measurements at different light intensities, the curves τ_d versus G (see Fig. 13) and the distribution of the $\tau_d^{(j)}$'s were obtained, as described in Sec. IV.

IV. DISCUSSION OF THE RESULTS AND CHECK OF THE THEORY

As stated in the Introduction, the measurements reported in Sec. III were performed to evaluate the parameters appearing in the theoretical expression of the power spectrum of the photoconductance noise worked out in Paper I. It will now be shown how such quantities can be determined from these data.

For convenience, the theoretical expression of the noise power spectrum is reported below:

$$\psi_G(\omega)=\frac{1}{G^2}\left[g\Delta g\tau_g\frac{\langle|S(\omega)|^2\rangle}{\tau_g^2}n_d + 2(\Delta g)^2\frac{|\langle S(\omega)\rangle|^2}{\tau_g^2}n_d\sum_j\frac{a^{(j)}\tau_d^{(j)}}{1+\omega^2\tau_d^{(j)2}}\right]. \tag{4.1}$$

In this equation g represents the contribution to the conductance G of a single electron in the conduction band, Δg is the average increase of conductance due to the excess ionization of a single deep donor center j (or of a single trapped hole) during its average lifetime $\tau_d^{(j)}$, and τ_g is the average lifetime of an electron in the conduction band related to thermally activated trapping-detrapping processes in shallow centers near the conduction band. The quantity $n_d=\sum n^{(j)}$ represents the total average number of the ionized centers or trapped holes and is proportional to the total positive trapped charge, while $n^{(j)}$ is the average number of ionized deep donor centers of type j, having a lifetime $\tau_d^{(j)}$ and a relative weight $a^{(j)}$. Finally, $\langle|S(\omega)|^2\rangle$ and $|\langle S(\omega)\rangle|^2$ are, respectively, the average square modulus and the square modulus of the average of the Fourier transform of a single conductance pulse of unitary amplitude, produced by the injection of an electron into the conduction band of the photoconducting material. As shown in Paper I, $|\langle S(\omega)\rangle|^2/\tau_g^2$ is practically a constant equal to $1/2\pi$ in the whole explored range of frequency, while $\langle|S(\omega)|^2\rangle/\tau_g^2$ shows at low frequencies the expected $1/f$ behavior and tends to the value $1/\pi$ at high frequencies.

According to Eq. (4.1), $\psi_G(\omega)$ is the sum of two different components having a different physical interpretation which helps in understanding their origin. The first component is related to the usual conduction fluctuation processes in a semiconductor, i.e., g-r plus $1/f$ noise. The second component is instead characteristic of the photoconduction mechanism and is related, according to the model described in Paper I, to the fluctuation of the height of the potential barrier which the electrons must overcome to be injected from the cathode into the conduction band of the photoconduction material. The height of this barrer is controlled by the positive space charge produced by light (ionized deep donor centers or trapped holes according to the value of λ) and by a feedback effect related to the negative space charge due to injected electrons (see Appendix B of Paper I). In Paper I, they have been called, respectively, *intrinsic* and *photoinduced* noise spectral components.

From the measurements reported in Sec. III, we can obtain all the parameters entering the expression of the photoinduced component and discuss their consistency with the experimental results. These parameters are τ_d, n_d, Δg, $\tau_d^{(j)}$, and $a^{(j)}$. Since the dependence of these parameters on light intensity and wavelength can be determined experimentally, the behavior of the noise spectrum as a function of these quantities is obtained without the introduction of any adjustable parameter when the photoinduced component is much larger than the intrinsic one. With regard to the intrinsic component, which contains the quantities τ_g and $\langle|S(\omega)|^2\rangle/\tau_g^2$, depending on the electron lifetime distribution function, a discussion is given afterwards.

The average relaxation constant τ_d, defined as the ratio between the total area of the relaxation pulse and its peak amplitude, can be measured with the technique described in Sec. II. The results of Fig. 13, concerning the behavior of τ_d versus G for $\lambda=510$ and 490 nm, were obtained from a large set of relaxation curves, like those of Fig. 11, obtained at different conductance values by varying the light intensity.

From Eq. (4.1), taking into account the results reported in Fig. 8, the values of η_λ reported in Sec. III, and the curve of τ_d versus G, the quantity n_d versus G was obtained (Fig. 14). According to the photoconduction model developed in Appendix B of Paper I, the curve n_d versus G should be independent of λ, since the conductance depends only on the net charge existing in the photoconductor. This is what actually happens, as shown by Fig. 14. This curve is also reported in the same Appendix B and compared with the theoretical one to show that the barrier-type photoconduction model is in good quantitative agreement not only with the noise but also with the behavior of the photoconductance versus light intensity in an extended range of values.

The first derivative of the curve reported in Fig. 14 provides the value of the quantity Δg appearing in Eq. (4.1) (Fig. 15). It is interesting to note that at high illumination values, Δg tends to a constant value. According to the model, it is expected that at high illumination values, $\Delta g\rightarrow g$, since the effect of the positive charge tends to be compensated by the negative charge due to the electrons in the conduction band. From Eq. (3.17), taking into account that $d\approx 1$ mm and the electron mobility is $\mu\approx 3\times10^{-2}$ m^{2}V^{-1}s^{-1},[4] it turns out that

$$g=\frac{e\mu}{d^2}\approx 5\times10^{-15}S\ , \tag{4.2}$$

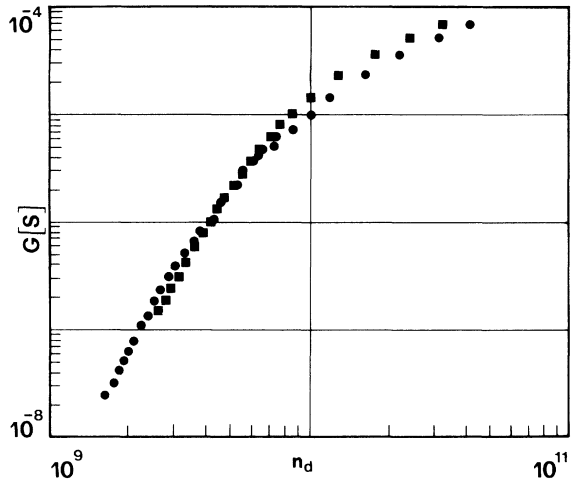

FIG. 14. The average conductance G at $\lambda=490$ nm (●) and at $\lambda=510$ nm (■) as a function of the total averge number of ionized deep donor centers or trapped holes n_d. As expected from the theory, the curve of G versus n_d is independent of the light wavelength λ. It has been obtained using Eq. (3.1) and the data reported in Figs. 8, 9, and 13 to evaluate n_d at different values of the conductance G.

which is of the correct order of magnitude, as the results of Fig. 15 show.

Finally, to make a good check of Eq. (4.1), the distribution of $\tau_d^{(j)}$'s must be obtained. According to the model, the nonexponential decay of the photocurrent pulse (Fig. 11) is attributed to a superposition of exponential pulses characterized by a time constant $\tau_d^{(j)}$ and a relative magnitude $h^{(j)}$. The relation between $h^{(j)}$ and $a^{(j)}$ can be obtained by taking into account Eqs. (I3.26), (I3.27), and (I3.35). One finds

$$a^{(j)}=\frac{b^{(j)}\tau_d^{(j)}}{\tau_d}=\frac{h^{(j)}\tau_d^{(j)}}{h\tau_d}\ , \tag{4.3}$$

h being the height of the photoconductance relaxation pulse.

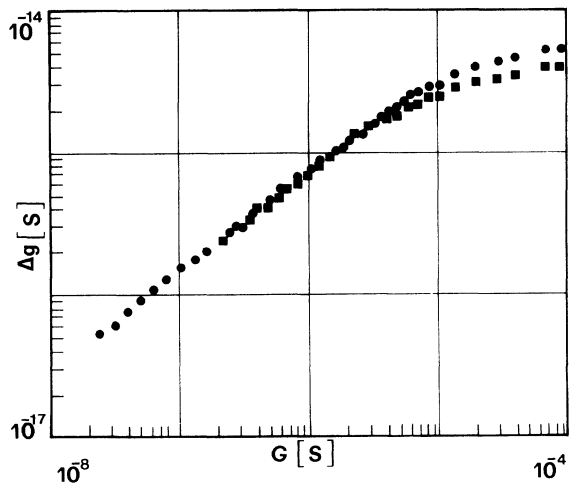

FIG. 15. The average conductance derivative with respect to n_d as a function of the average conductance G at $\lambda=490$ nm (●) and at $\lambda=510$ nm (■). This quantity has been directly obtained from the data of Fig. 14. The quantity Δg enters the theoretical expression of the power spectrum and, according to the model, tends to g for high light intensities. The dependence of the photoinduced noise component on $(\Delta g)^2$ is the origin of its more rapid drop with respect to the intrinsic one when the light intensity is decreased.

Such a distribution can be obtained by fitting either the decay with a discrete number of exponentials or the photoresponse curves (as those shown in Fig. 12) with the Fourier transform of a sum of exponentials whose time constants and amplitudes are set as best-fit parameters. This second procedure has proved to be the best one, since, by using the technique briefly described in Sec. III, very reliable photoresponse curves, down to very low frequencies, can be obtained. The best fit was performed by means of a suitable numerical procedure, using three exponentials at each value of λ. In order to get the whole set of the $\tau_d^{(j)}$ and $a^{(j)}$ needed to obtain the theoretical curves given in Figs. 6 and 7, in a wide range of G values, an interpolation procedure has been used. With regard to the spectra of Figs. 4 and 5, the sets of $\tau_d^{(j)}$ and $a^{(j)}$ values are given in Table I.

This procedure is similar to the dual-beam modulation spectroscopy (see for example Ref. 6 and references therein). However, it should be stressed that in the present case the method is suitable only for a check of the theoretical noise power spectrum [Eq. (4.1)] and that it is not reliable for the determination of the actual time constant distribution of the j centers. Different distributions, reproducing the photoresponse curve in a given frequency range, give very nearly the same results when introduced into Eq. (4.1), as can be proved by numerical evaluation.

Since, as already stated, the dimensionless quantity $|\langle S(\omega)\rangle|^2$, is practically a constant equal to $1/2\pi$ in the whole range of considered frequencies (10 Hz to 100 kHz), the power spectrum of the photoinduced noise component, which is the second term in the expression of $\psi_G(\omega)$, can be evaluated without introducing any other parameter. At photon flux densities larger than 10^{11} photons $s^{-1}\,cm^{-2}$ and at frequencies lower than 5 kHz, this spectral component turns out to be almost one order of magnitude larger than the intrinsic one, which is represented by the first term in Eq. (4.1). Thus, it can be stated that in these conditions the experimental data are in very good agreement with the theory also for what concerns absolute values, as shown in Figs. 6 and 7.

At higher frequencies or at lower photon flux densities, the intrinsic noise component becomes more and more important. The quantities τ_g and $\langle|S(\omega)|^2\rangle/\tau_g^2$ depend on the distribution of the electron lifetimes $P_2(\langle\tau_g\rangle)$ given by Eq. (3.2), and their expressions are worked out in Appendix A of Paper I. The distribution $P_2(\langle\tau_g\rangle)$ is characterized by K_1, which determines the ratio between the amplitudes of the $1/f$ to the g-r noise component, and τ_s, which is related to the cutoff frequency of the g-r noise Lorentzian spectrum.

These two quantities do not depend on the light intensity and, with respect to τ_s, nor do they depend on the

TABLE I. Values of lifetimes $\tau_d^{(j)}$ and of their relative weight $a^{(j)}$ as obtained according to the technique described in Sec. IV. Light wavelength and conductance values correspond to those of the noise spectra reported in Figs. 4 and 5.

Photoconductance		$G=2\times10^{-7}S$	$G=2\times10^{-5}S$
$\lambda=510$ nm	$\tau_d^{(1)}=400$ ms	$a^{(1)}=0.800$	$a^{(1)}=0.777$
	$\tau_d^{(2)}=40$ ms	$a^{(2)}=0.198$	$a^{(2)}=0.216$
	$\tau_d^{(3)}=4$ ms	$a^{(3)}=0.002$	$a^{(3)}=0.007$
$\lambda=490$ nm	$\tau_d^{(1)}=100$ ms	$a^{(1)}=0.482$	$a^{(1)}=0.396$
	$\tau_d^{(2)}=10$ ms	$a^{(2)}=0.462$	$a^{(2)}=0.504$
	$\tau_d^{(3)}=1$ ms	$a^{(3)}=0.056$	$a^{(3)}=0.1$

light wavelength. K_1 can be obtained from the experimental noise spectra taken at very low photon fluxes, where the intrinsic noise component dominates and the power spectrum becomes $1/f$ shaped at low frequencies. It is related to the angular frequency ω_c, where the $1/f$ and the g-r noise component intersect each other [Eq. (IA8)]. ω_c turns out to be 5×10^4 s^{-1} at $\lambda=510$ nm and 2.5×10^5 s^{-1} at $\lambda=490$ nm, independently of the light intensity. As already discussed in Sec. III, the increase of ω_c at $\lambda=490$ nm corresponds to the increase of the amplitude of the $1/f$ noise. This fact can be explained by observing that electrical conduction occurs mainly at the photoconductor surface, since the absorption coefficient has an abrupt increase for wavelengths shorter than λ_{gap}. The value of τ_s which gives a best fit of the experimental spectra up to 100 kHz for every wavelength and light intensity is equal to 8×10^{-8} s. This value is in good agreement with those found in the literature.[5]

V. CONCLUSIONS

In this paper we have reported an extended set of measurements concerning photoconductance, photoresponse, and noise power spectra carried out at different wavelengths above and below λ_{gap} in a wide range of photoconductance values. All these measurements were performed on the same device to check the photoconductance model and the theory of current noise developed in Paper I. The main results reported in Secs. III and IV can be summarized as follows.

(a) The relative variations of the shape and of the amplitude of the noise power spectra with light intensity and wavelength are reproduced by the theory without free parameters.

(b) At medium up to high light intensities ($\Phi_{n_f}>10^{11}$ photons s^{-1} cm^{-2}), the low-frequency part of the noise power spectrum (up to about 5 kHz), is dominated by the photoinduced noise component and can be evaluated from the theory without introducing any free parameters.

(c) The flattening of the spectrum at higher frequencies is due to the contribution of the intrinsic noise spectral component, which contains quantities such as τ_g and $\langle|S(\omega)|^2\rangle/\tau_g^2$, depending on the lifetime distribution of the electrons in the conduction band of the photoconducting material. At low light intensities ($\Phi_{n_f}\ll10^{11}$ photons s^{-1} cm^{-2}), this component dominates at low frequency and the power spectrum becomes $1/f$ sloped. At higher frequencies the spectrum again flattens, in agreement with the presence of a g-r noise component.

In this case, in order to calculate the noise power spectrum from Eq. (4.1), the parameter ω_c, which is related to the free-electron lifetime distribution, is needed. It corresponds to the angular frequency where the $1/f$ component intersects the flat g-r noise spectrum and determines the ratio between the amplitudes of the $1/f$ and g-r noise components. This parameter is obtained from the experimental spectra at very low illumination values and depends on λ near λ_{gap}, while it does not change when the light intensity is varied within the range used in these experiments. By using the value of ω_c obtained in this way and assuming a suitable value of τ_s, whose inverse represents the cutoff angular frequency of the g-r noise Lorentzian component, the whole set of the experimental spectra, for any value of the light intensity and wavelength, is well reproduced by Eq. (4.1) within the explored frequency range. Finally, as shown in Appendix B of paper I, the data fitting the experimental noise spectra by means of Eq. (4.1), also explain the behavior of photoconductance versus light intensity and wavelength for more than three orders of magnitude of photoconductance values.

[1]R. W. Smith, Phys. Rev. **97**, 1525 (1955).

[2]A. Carbone, F. Demichelis, and P. Mazzetti, in *Optical Materials: Processing and Science*, edited by D. B. Poker and C. Ortiz, MRS Symposia Proceedings No. 152 (Materials Research Society, Pittsburgh, 1989), p. 163.

[3]R. H. Bube, *Photoconductivity of Solids* (Wiley, New York, 1964).

[4]*Data in Science and Technology: Semiconductors*, edited by O. Madelung (Springer-Verlag, Berlin, 1992).

[5]R. H. Bube, *Photoelectronic Properties of Semiconductors* (Cambridge University Press, Cambridge, England, 1992).

[6]J. Bullot, P. Cordier, and M. Gauthier, Philos. Mag. B **67**, 751 (1993).

[7]A. Carbone and P. Mazzetti, preceding paper, Phys. Rev. B **49**, 7592 (1994).